Original Research Article

Multi-target UAV miniature staring hyperspectral imager radiation correction

Changchun Li[1*], Yanjie Wang[1], Chunyan Ma[1], Xiaoxiao Ma[2], Shuangting Wang[1]

[1*] *Henan University of Technology, Jiaozuo 454000, Henan province, China. E-mail: lichangchun610@126.com*

[2] *Zhengzhou Information Technology Vocational College, Zhengzhou 450008, Henan province, China.*

ABSTRACT

The micro staring hyperspectral imager can simultaneously acquire two spatial and one spectral images, and only record the external orientation elements of the entire hyperspectral image rather than the external orientation elements of each frame of the image, which avoids the geometric instability during scanning, effectively solves the problem of large geometric deformation of the small line scanning hyperspectral imager, and is suitable for the small UAV load platform with unstable attitude. At present, most of the research focuses on the radio-metric correction method of line scan hyperspectral imager. The application time of staring hyperspectral imager is short, and there is no mature data processing re-search at home and abroad, which hinders the application of UAV micro staring hyperspectral imaging system. In this paper, the calibration method of the linearity and variability of the radiation response of the micro staring hyperspectral imager on the UAV is studied, and the effectiveness of this method is quantitatively evaluated. The results show that the hyperspectral image has obvious vignetting effect and strip phenomenon before the correction of radiation response variability. After the correction, the radiation response variation coefficient of pixels in different bands decreases significantly, and the vignetting effect and image strip decrease significantly. In this paper, a multi-target radiometric calibration method is proposed, and the accuracy of radiometric calibration is verified by comparing the calibrated hyperspectral image spectrum with the measured ground object spectrum of the ground spectrometer. The results show that the calibration results of the multi-target radiometric calibration method show better results, especially for the near-infrared band, and the difference with the surface reflectance measured by the spectrometer is small.

Keywords: Micro Staring Hyperspectral Imager; Line Scan Hyper-Spectral Imager; Radiation Response Linearity; Radiation Response Variability; Spectral Calibration; Radiometric Calibration

ARTICLE INFO

COPYRIGHT

1. Introduction

In recent years, UAV hyperspectral imaging technology has been gradually popularized in some research and application fields, and it has been more and more widely used in environmental monitoring and protection, disaster monitoring and assessment, geological exploration, urban planning and other fields[1-6]. Traditionally, hyperspectral imagers are often carried on aviation or satellite platforms. Due to the long repetition period and low spatial resolution of satellite platforms, as well as the high cost of image acquisition on aviation platforms, the application of aviation and satellite hyperspectral imaging technology is hindered[7]. With the emergence of new low altitude platforms such as small UAVs and micro hyperspectral imaging sensors, hyperspectral remote sensing data acquisition methods are changing rapidly[8].

At present, the main types of hyperspectral imagers are wire scanning and staring. The line scan hyperspectral imager uses a two-

dimensional detector array to obtain only one spatial dimension and one spectral dimension image. Since only one row or column of images are obtained each time, the geometric quality of the image is extremely sensitive to the rotation and vibration of the load platform. The unstable UAV platform will cause large geometric deformation of the hyperspectral image[9,10]. The staring hyperspectral imager can obtain two spatial dimensions and one spectral dimension image at the same time to form two spatial dimension images with dozens to hundreds of bands. It only needs to record the external orientation elements of the entire hyperspectral image without recording each frame, thus avoiding the geometric instability during scanning operation. Therefore, the small staring hyperspectral imager can effectively solve the problem of large geometric deformation of small line scanning hyperspectral imager imaging on UAV, and is suitable for load platforms with unstable attitude, such as small UAV.

Compared with the line scan hyperspectral imager, the staring hyperspectral imager has a shorter application time, and there is no mature data acquisition, processing and application research at home and abroad, which makes the application of the staring hyperspectral imager system of UAV face certain obstacles.

This paper evaluates the image quality from the aspects of the radiation response linearity and radiation response variability of the micro staring hyperspectral image of the UAV, and tests the wavelength calibration deviation, radiation response linearity of the staring hyperspectral imager and the radiation response variability of the hyperspectral sensor CCD. This paper focuses on the method of eliminating the variability of the radiation response of the micro staring hyperspectral image of the UAV, and quantitatively evaluates the effectiveness of this method. A radiometric calibration method based on multi-target hyperspectral images is proposed, and the radiometric calibration accuracy is verified by comparing the hyperspectral image spectra after calibration with the ground object spectra actually measured by the ground spectrometer.

2. Test equipment and data acquisition

The UAV carrier platform adopts Dajiang tumbling cloud S1000 + eight rotor UAV, and the imager is UHD 185 micro staring hyperspectral imager. The imager includes 138 spectral bands with a sampling interval of 4 nm. HG-1 mercury argon spectral calibration lamp is selected as the light source for spectral calibration. The fieldSpec Pro FR spectrometer is selected to measure the spectral curve of the ground calibration object and each research area.

When acquiring hyperspectral image data of field UAV, 5 pieces of grey cloth, green cloth, red cloth, blue cloth and black cloth with rough surface and size of 1.5 m × 1.5 m, which are close to Lambertian body, are respectively arranged in the flight route of UAV. Before the flight operation of UAV, ASD spectrometer is used to measure the reflectivity curve of these rough cloth blocks. The flight altitude of the UAV is 50 m, the speed is 5 m/s, and the image course overlap and side overlap are set to 70% and 60%, respectively.

3. Spectral calibration and radiometric calibration of hyperspectral images

3.1 Hyperspectral image spectral calibration

Spectral calibration is the process of determining the central wavelength position and spectral bandwidth of each band in hyperspectral images. Although the spectrometer has been calibrated before leaving the factory, its wavelength will change with time and use environment. In addition, the spectral calibration results can be used to simulate the FWHM (full width at half maximum) of each band to determine the spectral resolution of the hyperspectral sensor.

For the spectral calibration of UHD 185 hyperspectral spectrometer, firstly, place the spectrometer under the HG-1 mercury argon spectral calibration lamp and collect the spectral curve of hyperspectral cube to determine the band number of all peaks of the curve. Then, find the spectral lines of mercury argon spectral calibration lamp corresponding to all peaks of the curve to determine the spectral wavelength value of each peak. Finally, a linear or polynomial function between the wave-

length of the spectral curve of the light source and the serial number of the corresponding peak of the hyperspectral cube spectral curve is constructed, and the wavelength of each band is calculated by using the linear function with the serial number of the band as the independent variable. The linear function is

$$\lambda_i = \lambda_0 + \alpha i, \quad i = 1, 2, 3, \ldots, n \tag{1}$$

Where, i is the serial number of each band; λ_i is the wavelength of band i; λ_0 is the wavelength of the first band; α is the coefficient. The number of samples tested in the laboratory is generally greater than 2, and λ_i and α are calculated by the least square method.

3.2 Calculation of radiation response linearity

The radiation response linearity is ed by the linear relationship between the DN value of the image and the incident spectral radiation intensity measured by the integrating sphere. The calculation equation is[11]

$$\hat{Y} = \text{gain}_i \times \text{DN}_i + \text{offset}_i, \quad i = 1, 2, 3, \ldots, 125 \tag{2}$$

$$L_i = \sum_i^n \frac{(Y_i - \hat{Y}_i)}{(\sum_i^n Y_i)^2} - \sum_i^n (Y_i)^2 / n, \quad i = 1, 2, 3, \ldots, 125 \tag{3}$$

Where DN_i is the average DN value of the ith band of hyperspectral cube; gain_i and offset_i are the coefficients of the model, that is, the gain value and offset value of each band; $\hat{Y}$ and Y_i are the estimated spectral radiance and the spectral radiance recorded by the spectrometer respectively; n is the number of samples.

Using equation (2), the DN value of each gradient of the image is taken as the independent variable, and the spectral radiation intensity measured by the optical integrating sphere is taken as the dependent variable. The DN value and radiation intensity value of 18 groups of images measured in the test are fitted through the least square linear model to obtain the gain value and offset value of each band. Equation (3) represents the determination coefficient R^2 of the fitting result of equation (2), which is used to characterize the linearity of radiation response.

3.3 Radiation response variability and correction

Affected by the instrument noise, vignetting effect and other sensor related factors, hyperspectral cube images will have certain variability in radiation response[12,13]. Before hyperspectral image processing and application, it is necessary to correct the variability of hyperspectral cube radiation response in advance. In order to correct the variability of radiation response, the ratio of two images obtained at the same wave band under different irradiation intensities is used, and the influence of dark current is subtracted before calculating the ratio. This method assumes that the radiation response of each pixel is linear. This process can be represented by equation (4). One of the two images is used as the reference image and the denominator of equation (4).

$$R_{i,j,\lambda} = (\text{DN}_{i,j,\lambda} - \text{DC}_{i,j,\lambda}) / (\text{DN}_{i,j,\lambda}^c - \text{DC}_{i,j,\lambda}) \tag{4}$$

Where $\text{DN}_{i,j,\lambda}$, $\text{DN}_{i,j,\lambda}^c$ and $\text{DC}_{i,j,\lambda}$ are respectively the λ band DN value, reference hyperspectral cube image and dark current value; i, j, λ are respectively the row number, column number and wavelength of image pixels.

The variation degree of radiation response is quantitatively calculated by the following equation:

$$I_\lambda = v_\lambda / m_\lambda \tag{5}$$

Where, I_λ is the variation coefficient of radiation response; v_λ and m_λ are the variance and mean of the band DN at wavelength λ, respectively.

3.4 Hyperspectral image radiometric calibration

The purpose of image radiometric calibration is to convert the DN value of the cube image obtained by UHD 185 hyperspectral imager into radiance or reflectivity, and eliminate or weaken the radiation deviation caused by the sensor itself and atmospheric factors[14,15]. In this paper, two radiometric calibration methods are studied. The first is single target radiometric calibration method (see equation (6)), which multiplies the relative reflectance of hyperspectral images relative to the white calibration plate photographed on the ground by the absolute reflectance of the white calibration plate to

obtain the absolute reflectance of each band. Because the hyperspectral cube image of the white reference plate is obtained on the ground surface, and the hyperspectral image is obtained on the UAV, the influence of the sensor and the atmosphere cannot be eliminated when the single target radiometric calibration method is used for radiometric calibration. In this paper, another multi-target radiometric calibration method (see equation (7)) is studied. This method, combined with the image radiometric variability correction algorithm, can restrain the radiation distortion caused by sensor and atmospheric factors.

$$\mathrm{Ref}_{i,j,\lambda} = \mathrm{MR}_{i,j,\lambda} \times \mathrm{Ref}_w \tag{6}$$

$$\mathrm{Ref}_{i,j,\lambda} = \mathrm{MR}_{i,j,\lambda}/\mathrm{mean}(\mathrm{MR}_\lambda^w) \times \mathrm{Ref}_w \tag{7}$$

Where, $\mathrm{Ref}_{i,j,\lambda}$ is the reflectance after radiometric calibration; Ref_w is the reflectance of the reference object. In this paper, the reference object is white cloth laid on the ground, and its reflectance is measured by ASD spectrometer; $\mathrm{MR}_{i,j,\lambda}$ is the DN value of the image after the radiation response variability correction; mean (MR_λ^w) is the average value of the pixel DN of the reference object; i, j represents the row and column number of the image.

4. Results and analysis

4.1 Calculation results and characteristics of radiation response linearity

Use equations (2) and (3) to calculate the radiation response linearity of all bands of UHD 185 hyperspectral imager, and the results are shown in **Figure 1**.
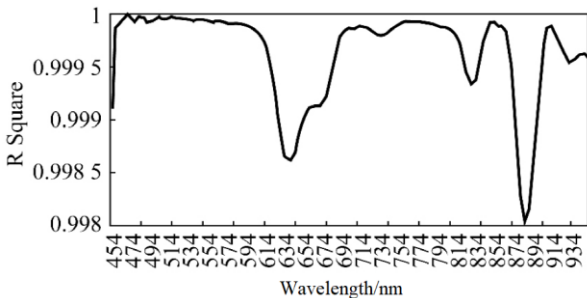
Figure 1. Radiation response linearity of UHD 185 Hyperspectral imager in all bands.

It can be seen from **Figure 1** that the radiation response linearity of UHD 185 hyperspectral imager exceeds 0.998 in all bands, which is the prem-

ise for UHD 185 hyperspectral imager to achieve good radiation calibration results. However, the radiation response linearity of different bands is unstable and fluctuates greatly. At 470–610 nm, 694 and 895 nm, the spectral radiation response linearity is significantly higher than that of other bands. However, there are obvious valleys around 454, 638 and 882 nm.

4.2 Radiation response variability correction

Figure 2 and **Figure 3** respectively show the variation of image pixel values before and after the correction of radiation response variability at 550 nm band and the histogram of frequency distribution before and after the correction. **Figure 4** shows the situation before and after the correction of the radiation response variation coefficient of all bands. In **Figure 4**, I1 and I2 represent the radiation response variation coefficient of each band of the original image taken at the integrating sphere outlet under different radiation brightness conditions, (l1-DC)/(l2-DC) represents the radiation response variation coefficient of the corrected image.

From **Figure 2** to **Figure 4**, it can be seen that before the radiation response variability correction, the radiation response variation coefficient of the image is large, and there is obvious vignetting effect and strip phenomenon. After the radiation response variability correction, the radiation response variation coefficient of pixels in different bands is significantly reduced, and the radiation variation coefficient of all bands is less than 0.01, and the vignetting effect and image strip are significantly reduced. It shows that the method proposed in this paper can effectively correct the radiation response variability of images.

4.3 Radiometric calibration and accuracy analysis

The single target radiometric calibration method represented by equation (6) and the multi-target radiometric calibration method represented by equation (7) are used for radiometric calibration respectively, and the reflectance of green cloth and celery is selected for calibration effect evaluation. The results are shown in **Figure 5a** and **Figure 5b**. In **Figure 5**, C1 is the calibration result of sin-

(a) Before correction
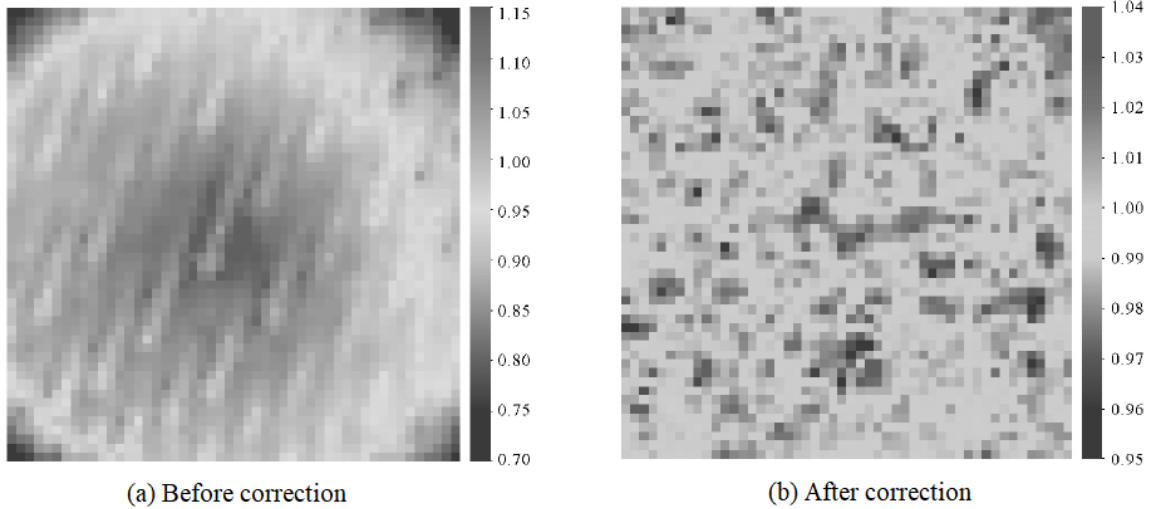
(b) After correction

Figure 2. Image pixel values before and after correction of radiation response variability at 550 nm band.

(a) Before correction
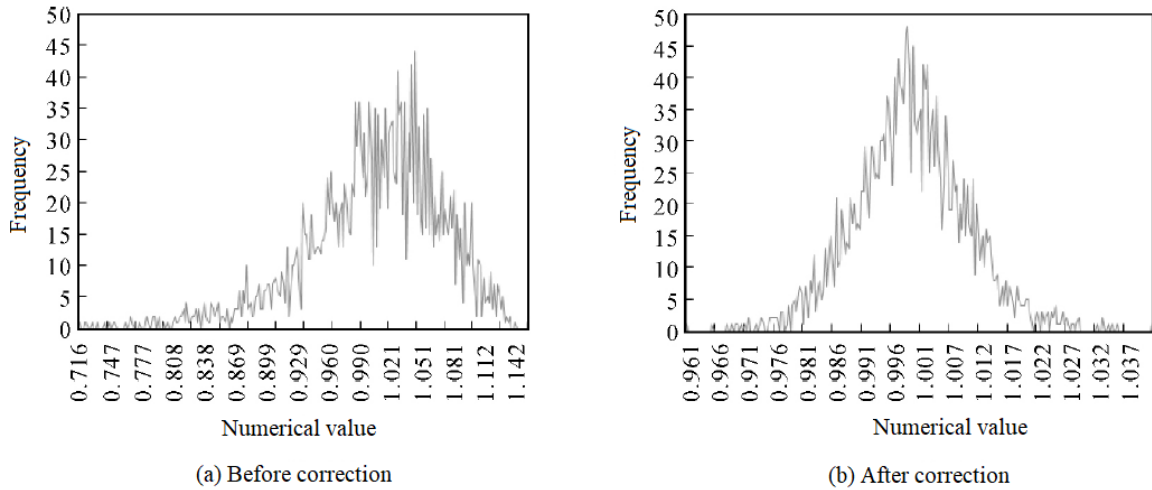
(b) After correction

Figure 3. Frequency distribution of image before and after correction of radiation response variability at 550 nm band.
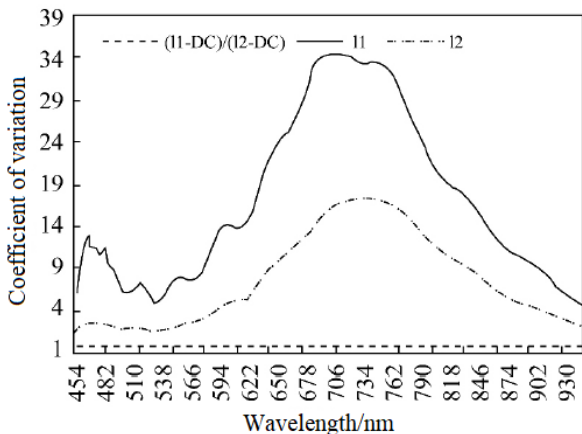
Figure 4. Radiation response variation coefficient of all bands before and after correction.

gle target radiometric calibration method, C2 is the calibration result of multi-target radiometric calibration method, and ASD is the measured result of spectrometer.

From the above calibration results, it can be known that: (1) the multi-target radiometric calibration method represented by equation (7) shows better calibration effect, especially for the near-infrared band, and the difference with the surface reflectance measured by ASD spectrometer is small. The single target radiation calibration method represented by equation (6) is used for calibration, which shows that the surface reflectance is significantly lower than that measured by the ASD spectrometer in the near-infrared region of the 722 ~ 950 nm spectral range, and the reflectance drops rapidly after 882 nm, which is not in line with the change trend of the actual surface reflectance.

(2) The calibration results of multi-target radiometric calibration method are compared with the measured spectral curve of ASD spectrometer. The results show that for the green cloth, the measured spectral curve of ASD spectrometer can see small

36

oxygen absorption characteristics near 760 nm, and the oxygen absorption characteristics of the image are no longer obvious after radiometric calibration. In the 910 ~ 950 nm spectral range, the difference between the radiometric calibration results and the measured results of ASD spectrometer is less than 5%, and in the 500 ~ 950 nm spectral range, the difference between the two is less than 4%; for celery, the difference is less than 3% in the 458 ~ 910 nm spectral range, and less than 4% in the 910 ~ 950 nm spectral range.
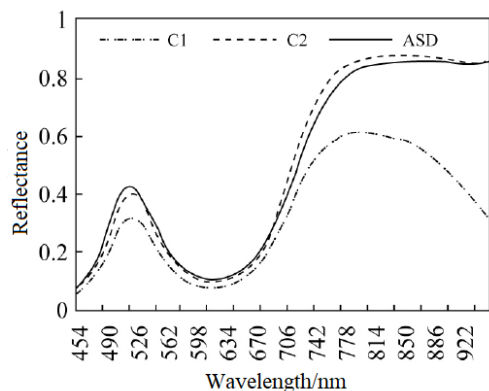
(a) Reflectance of green cloth after radiation calibration
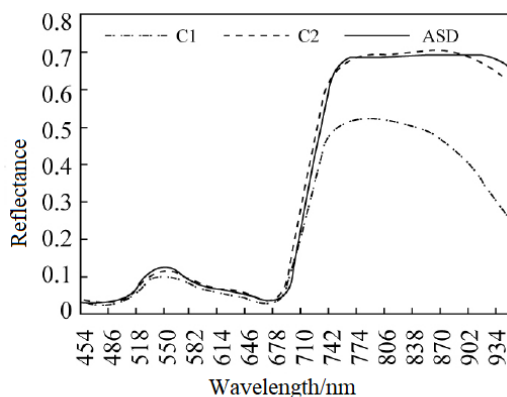
(b) Reflectance of celery after radiation calibration

Figure 5. Different radiation calibration results of green cloth and celery.

5. Conclusion

At present, UAV micro staring hyperspectral remote sensing system is a relatively new low altitude remote sensing platform, which can obtain hyperspectral remote sensing data flexibly, quickly and reliably. The experimental results show that the CCD of UHD 185 staring hyperspectral imager has certain spectral calibration deviation, and has obvious vignetting effect and fringe phenomenon, which seriously affects the image quality and is not suitable for direct quantitative analysis and application. Firstly, the original hyperspectral image is corrected for the variability of the radiation response. After correction, the image quality is significantly improved and the variability of the radiation response is obviously eliminated, and there is no obvious vignetting effect and fringe phenomenon. At the same time, the single target and multi-target radiometric calibration methods are studied in this paper. The results show that, compared with the single target radiometric calibration method, the multi-target radiometric calibration method achieves better calibration results, especially can significantly improve the problem of reflectance reduction in the near-infrared spectral region.

Conflict of interest

The authors declare that they have no conflict of interest.

References

1. Mulla DJ. Twenty five years of remote sensing in precision agriculture: Key advances and remaining knowledge gaps. Biosystems Engineering 2013; 114(4): 358–371.
2. Zhang C, Kovacs JM. The application of small unmanned aerial systems for precision agriculture: A review. Precision Agriculture 2012; 13(6): 693–712.
3. Habib A, Han Y, Xiong W, *et al*. Automated orthorectification of UAV-based hyperspectral data over an agricultural field using frame RGB imagery. Remote Sensing 2016; 8(10): 796.
4. Schima R, Mollenhauer H, Grenzdorffer G, *et al*. Imagine all the plants: Evaluation of a light-field camera for on-site crop growth monitoring. Remote Sensing 2016; 8(10): 823.
5. Feng W, Zhang HY, Zhang YS, *et al*. Remote detection of canopy leaf nitrogen concentration in winter wheat by using water resistance vegetation indices from in-situ hyperspectral data. Field Crops Research 2016; 198: 238–246.
6. Contiu S, Groza A. Improving remote sensing crop

classification by argumentation-based conflict resolution in ensemble learning. Expert Systems with Applications 2016; 64: 269–286.

7. Tong Q, Zhang B, Zhang L. Zhongguo Gaoguangpu Yaogan de qianyan yu jinzhan (Chinese) [The frontier and progress of hyperspectral remote sensing in China]. National Remote Sensing Bulletin 2016; 20(5): 689–707.

8. Zhang C, Xiang Y. Jiyu daqi xishoudai de chaoguangpu chengxiangyi guangpu dingbiao jishu yanjiu (Chinese) [Study on spectral calibration technology of hyperspectral imager based on atmospheric absorption band]. Spectroscopy and Spectral Analysis 2012; 32(1): 268–272.

9. Bi K, Li Y, Ding X, *et al*. Qingxiaoxing wurenji hangshe jishu xianzhuang ji fazhan qushi (Chinese) [Present situation and development trend of aerial photography technology for light UAV]. Bulletin of Surveying and Mapping 2015; (3): 27–31, 48.

10. Lin Z, Xie W, Su G. Kuanjiao xiangji dikong zehang de jingdu fenxi (Chinese) [Measurement accuracy analysis of wide-angle camera at low altitude]. Acta Geodaetica et Cartographica Sinica 2014; 43(10): 991–997.

11. Karpel N, Schechnery Y. Portable polarimetric underwater imaging system with a linear response. Proceedings of SPIE 2004; 5432: 106–115.

12. Zheng Y, Yu J, Kang S, et al. Single-image vignetting correction using radial gradient symmetry. 2008 IEEE Conference on Computer Vision and Pattern Recognition; 2008 Jun 23–28; Anchorage, AK, USA. New York: IEEE; 2008.

13. Goldman DB, Chen JH. Vignette and exposure calibration and compensation. Tenth IEEE International Conference on Computer Vision; 2005 Oct 17-20; Beijing. New York: IEEE; 2005.

14. Zhang Z, Zhang H, Chang Y, *et al*. Landsat xilie weixing guangxue yaogan fushe dingbiao fangfa zongshu (Chinese) [Summary of radiometric calibration methods for Landsat series satellite optical remote sensors]. National Remote Sensing Bulletin 2015; 19(5): 719–732.

15. Han J, Xie Y. Xingzai duoxiangji pinjie chengxiang chuanganqi zaigui fushe dingbiao fangfa (Chinese) [On orbit radiometric calibration method for spaceborne multi camera mosaic imaging sensor]. Acta Geodaetica et Cartographica Sinica 2017; 46(11): 1830–1840.

16. Zhang G, Li L. Yaogan 25 hao wuchanghua xiangdui fushe dingbiao (Chinese) [Remote sensing 25 unfield relative radiometric calibration]. Acta Geodaetica et Cartographica Sinica 2017; 46(8): 1009–1016.